
# Investigation of biomass alkali release in a dual circulating fluidized bed chemical looping combustion system

Downloaded from: https://research.chalmers.se, 2025-12-04 23:34 UTC

Citation for the original published paper (version of record):

Gogolev, I., Pikkarainen, T., Kauppinen, J. et al (2021). Investigation of biomass alkali release in a dual circulating fluidized bed chemical looping
combustion system. Fuel, 297. http://dx.doi.org/10.1016/j.fuel.2021.120743

N.B. When citing this work, cite the original published paper.

research.chalmers.se offers the possibility of retrieving research publications produced at Chalmers University of Technology. It covers all kind of research output: articles, dissertations, conference papers, reports etc. since 2004. research.chalmers.se is administrated and maintained by Chalmers Library

(article starts on next page)

Fuel 297 (2021) 120743

Contents lists available at ScienceDirect

Fuel

journal homepage: www.elsevier.com/locate/fuel

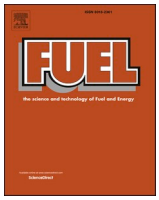

Full Length Article

# Investigation of biomass alkali release in a dual circulating fluidized bed chemical looping combustion system

Ivan Gogolev [a,*], Toni Pikkarainen [b], Juho Kauppinen [b], Carl Linderholm [a], Britt-Marie Steenari [a], Anders Lyngfelt [a]

[a] Chalmers University of Technology, Sweden
[b] VTT Technical Research Centre of Finland, Sweden

ARTICLE INFO

*Keywords:*
Chemical looping combustion
Alkali
Biomass
Oxygen carriers

ABSTRACT

Chemical looping combustion (CLC) of biomass is a promising technology for power generation with integrated carbon capture. In CLC, alkali content of biomass poses potential issues of bed agglomeration, as well as heat exchanger fouling and corrosion. The fate of biomass alkalis was investigated in a dual-interconnected circulating fluidized bed CLC system. Experiments were conducted in oxygen carrier aided combustion (OCAC) and CLC modes. Ilmenite and braunite oxygen carriers and three biomass fuels (wood pellets, wood char, straw pellets) were tested. Flue gas alkali emissions in the air reactor (AR) and fuel reactor (FR) were measured with a surface ionization detector (SID). Results showed that CLC operation yields gas-phase alkali emissions that are up to 15 times higher than in comparable OCAC operation. Results analysis concluded that increased alkali emissions in CLC arise from the steam atmosphere in the FR, whereby steam accelerates the decomposition of alkali compounds in the biomass. Retention of alkalis in the condensed phase was found to be >97% for ilmenite and >92% for braunite CLC operation. Up to 60–80% of the retention was attributed to fuel ash formation. The residual retention was attributed to absorption of alkalis by the oxygen carriers. Absorption likely occurred mainly through formation of alkali manganates and silicates in braunite, and formation of alkali silicates, aluminosilicates, manganates, and titanates in ilmenite. Gas-phase alkali emissions in the AR, although less than in the FR, were found to occur due to combustion of unconverted fuel carried over from the FR to the AR.

## 1. Introduction

Chemical looping combustion (CLC) is a novel thermal fuel conversion technology with inherent carbon dioxide capture [1]. In CLC, an oxygen carrier (OC) material, typically a metal oxide, is circulated between two interconnected reactors. The OC is oxidized in the air reactor (AR) with air and is then conveyed to the fuel reactor (FR), where the OC undergoes reduction by fuel. Only the OC is circulated between the reactors, which allows delivery of oxygen to the fuel while nitrogen from the air leaves with the flue gas of the AR. The reduced OC from the FR is recirculated back to the AR for re-oxidation. Since fuel conversion in CLC occurs in the FR without the presence of nitrogen, the FR exhaust consists mostly of $CO_2$ and $H_2O$. In CLC, carbon dioxide capture is achieved without the need for costly and energy-intensive nitrogen separation. A more complete overview of the CLC technology can be found in review publications [2,3].

CLC technology was originally demonstrated with gaseous fuels [4], but has seen further development enabling the CLC principle to be applied to liquid and solid fuel conversion [5]. Currently, literature indicates that the collective CLC operating experience amounts to>11,000 h of CLC operation in 49 CLC pilot reactors ranging in scale from 300 $W_{th}$ to 1 $MW_{th}$ [3]. Recently, CLC of biomass fuels has gained interest in light of the increasing need to deploy negative emissions technologies (NETs) to combat climate change in the near future [6]. Utilizing biomass fuels in CLC presents several challenges. With respect to fuel conversion efficiency, biomass fuels are challenging as they typically have a high volatiles content which is rapidly released in devolatilization, as the fuel is introduced into the fuel reactor. Achieving full conversion of the volatiles is difficult. This typically requires optimizing the reactor design to maximize the contact between the volatiles and the oxygen carrier [7], as well as selection of more reactive OC materials, such as synthetic and natural material blends [8], or OC materials that are capable or releasing free oxygen in the FR [9].

Another critical but less explored issue in CLC of biomass fuels is the potential operational challenges that stem from the release of alkali

* Corresponding author.
*E-mail address:* gogolev@chalmers.se (I. Gogolev).

https://doi.org/10.1016/j.fuel.2021.120743
Received 21 November 2020; Received in revised form 13 February 2021; Accepted 19 March 2021
Available online 9 April 2021
0016-2361/© 2021 The Authors. Published by Elsevier Ltd. This is an open access article under the CC BY license (http://creativecommons.org/licenses/by/4.0/).

**Nomenclature**

| | |
|---|---|
| AR | air reactor |
| CLC | chemical looping combustion |
| CLOU | chemical looping with oxygen uncoupling |
| CPC | condensation particle counter |
| D-CFB | dual circulating fluidized bed |
| FR | fuel reactor |
| NETs | negative emissions technologies |
| OC | oxygen carrier |
| OCAC | oxygen carrier aided combustion |
| PDU | process development unit |
| SMPS | scanning mobility particle sizer |
| SID | surface ionization detector |
| SP | Straw pellets |
| WC | wood char |
| WP | wood pellets |
| $\eta_{oo}$ | oxide oxygen efficiency (%) |

metal compounds from biomass fuels during the fuel conversion process. In conventional fluidized bed combustion and gasification, alkalis released from biomass to the gas-phase are known to lead to fouling and corrosion of heat exchange equipment, while alkalis released to the non-volatile ash fraction are known to lead to bed material agglomeration [10,11]. In CLC, the effect of biomass alkalis is not well known, with only several studies reporting alkali emissions measurements from pilot operation [7,8]. The aim of the current work was to further develop the understanding of alkali release in CLC that was developed in previous studies [7,8]. Specifically, the experiments conducted in the present study aimed at determining how different oxygen carriers affect alkali release from fuel. Furthermore, this study aimed to establish how alkali release in CLC operation differs from conventional fluidized bed combustion processes.

## 2. Background

CLC of solid fuels was first demonstrated by Berguerand and Lyngfelt in 2008 [12]. Since then many more studies have successfully operated CLC pilot systems capable of converting solid fuels. A summary of development of solid-fuel CLC can be found in reference [13]. Chemical looping combustion of solid fuels, whether fossil or biomass-derived, is complicated by the fact that solid fuels need to decompose to gaseous species in order to react with the oxygen carrier. As solid fuel is introduced in the fuel reactor it is rapidly heated and undergoes staged decomposition. First, the volatile fraction is devolatilized, leaving behind solid char and inorganic matter. In order to convert the char, the FR is typically fluidized with steam or $CO_2$. Steam or $CO_2$ act as a gasification agent, converting the solid char to CO and $H_2$. Most of the inorganic matter present in the char forms fine fly ash that is elutriated, or larger bottom ash that stays with the bed material. The volatiles released in devolatilization and the gasification products generated from char gasification react with the oxygen carrier in a gas–solid reaction [14].

The composition of the fuel has significant influence on the overall fuel conversion process. Fossil fuels such as coal and coke tend to have a moderate volatiles content and thus a large residual char fraction. Due to the high char fraction, fuel conversion of fossil-derived solid fuels in CLC is typically limited by the slow char gasification step [13,15]. Also, fossil-derived solid fuels tend to have a large fraction of inorganic content which results in significant amounts of ash formation. Biomass fuels behave differently. Biomass fuels typically have a much higher volatiles content of 60–85 wt% [16]. Due to the high volatiles fraction and the fact that devolatilization is a fast process, fuel conversion of biomass in CLC is limited by the contact efficiency of the volatiles fraction with the OC. Contrary to fossil-derived solid fuels, char conversion in CLC of biomass is much more efficient. Firstly, because of the high volatiles fraction of biomass fuels, the char fraction is low. Secondly, biomass char is known to be more reactive. Biochar's increased reactivity is attributed to higher specific surface area and the presence of alkali species (K and Na) which are present in biomass fuels but are scarce in fossil-derived fuels. These alkali components have been shown to catalyse char gasification [17,18].

Experience from conventional fluidized-bed based thermal conversion technologies, mainly fluidized bed combustion and gasification, reveal that the biggest challenge of biomass fuel conversion in fluidized bed systems stems from the fuel's inorganic matter. Depending on the fuel type, the ash content can vary from $< 1\%$ in woody biomass to as high as 40% ash content in herbaceous biomass. The primary ash-forming species present in biomass are Si, Al, Fe, Ca, Mg, Na, K, and S [10]. While some of the inorganic species are relatively benign, major issues arise from alkali and chlorine (Cl) content. From the alkali species, potassium (K) and sodium (Na) are the most prevalent and are often found to be the most problematic species. As shown by selective leaching analyses of multiple biomass fuels, K and Na are present in biomass in different forms. Alkali species present in the fuel as excluded minerals arise mostly from contamination of fuel during processing. This form tends to be quite inert and does not have significant implications on thermal conversion [19]. Most of the K and Na in biomass is present as finely dispersed salt, in plant fluids, or in organically bound form. These alkali fractions are known to be effectively released during thermal conversion of the fuel. Typically, the amount of K present in biomass fuel is much higher than that of Na (up to $10\times$ more). Due to this dominance, and the fact that K and Na chemistry is similar, K release is often considered to be the most critical phenomenon. In combustion, the release of K occurs during the devolatilization and char burnout stages. Only $< 10\%$ of K is released at temperatures below 700 °C, mostly due to decomposition of the organically bound K. The remaining K release occurs at temperatures above 700 °C [10]. Most of the remaining K is released through sublimation of KCl to the gas phase. Further gas-phase release can occur from decomposition of alkali salts, such as $K_2CO_3$ and $K_2SO_4$. In the high-temperature release regime, release of K to the gas phase is counteracted by competing formation of K-silicates. In this process K forms non-volatile silicate compounds by reacting with silica that is present in the fuel or in the bed material. K-silicate formation acts to retain the K in the bottom ash or bed material fraction.

Both, release of K to the gas phase and retention of the K in the bottom ash, can have detrimental effects on the thermal conversion system's operation. In the bottom ash, alkali silicates that form via reaction of alkalis with $SiO_2$ can have melting point temperatures lower than 700 °C [22]. Since typical biomass-fueled furnaces operate at around 800–900 °C, some of the alkali silicate species form sticky melts that can cause the onset of bed agglomeration. With time, increasing agglomeration leads to defluidization and eventually results in unplanned unit shutdowns [10,16,20]. Operation of the furnace at lower temperatures can mitigate agglomeration, but would negatively impact process heat recovery, leading to overall lower system thermal efficiency. In practice, alkali induced agglomeration is usually dealt with by continuous removal of bottom ash and replacement of the bed material. Large scale commercial boilers can replace up to 1/3 of the total boiler inventory per day [14]. Other methods for combatting agglomeration include the use of alternative bed materials such as olivine, dolomite, ferrous oxide, feldspar, and blast furnace slag, or addition of materials that contain aluminum silicates (e.g. kaolin, or other clay minerals) which react with alkalis to form silicates with higher melting temperatures [21].

Alkalis released to the gas-phase contribute to fouling and corrosion of the heat exchange equipment in the convection pass of the boiler. Fouling occurs as alkali salts that are released to the gas phase begin to cool as they pass the heat exchange equipment. Cooling results in

condensation of the alkali salts into melt aerosol that sticks onto the surface of the heat exchange equipment. Once the heat exchange surface is wetted, further deposit growth occurs by impaction of condensed salts or impaction of other fly ash fractions [22]. The formed deposits impede heat transfer and lower overall thermal efficiency of the system. Extreme deposit growth necessitates installation of soot blowing equipment that can clear the deposits during boiler operation. Alternatively, extensive shut-down and maintenance periods are required to clear the deposits. Further to impeding heat transfer, heat exchanger deposits are known to cause high temperature corrosion which leads to material deterioration of the heat exchanger tubes. From the many possible deposited species, KCl is especially deleterious as it causes extreme high temperature corrosion [22]. Mitigation measures to fight formation of deposits and corrosion include strategies of co-firing biomass fuels with fuels with a high sulfur content, addition of elemental sulfur to the bed material, or injection of sulfur-containing chemicals into the flue gas of the boiler. Sulfur, or sulfur-containing species are able to reform KCl to $K_2SO_4$ and HCl. While $K_2SO_4$ can still participate in the formation of heat exchanger deposits, it is significantly less aggressive in terms of corrosion.

In CLC, the fate of fuel alkalis remains largely unexplored, with only two publications reporting alkali release measurements [7,8] from pilot operation. These studies show that in CLC, alkalis can be released to the gas phase in both the FR and AR. The distribution of the gas phase release was reported to be even for low-alkali biomass fuels, but higher in the FR for high-alkali fuels. It was also shown that the overall gas-phase release levels typically grow with the fuel's alkali content. The gas-phase alkali release measurements presented in these studies were performed in CLC operations where the OC was either 100% ilmenite, or a mixture of ilmenite and synthetic calcium manganite material. Since ilmenite is known to be effective in absorbing potassium through formation of potassium titanates, both studies concluded that ilmenite's affinity for alkalis made it difficult to determine how the nature of the two-reactor system used in the CLC scheme influences the release of alkalis from the fuel.

In the current study, operation was performed with ilmenite and braunite oxygen carriers. Braunite is a manganese ore with low titanium content. Braunite was expected to exhibit lower alkali absorption, and thus allow for more unincumbered determination on how the two-reactor CLC system affects alkali release and distribution. Further to operation with two different oxygen carriers, the current study attempted to determine how alkali release in a CLC system differs from conventional fluidized bed biomass boilers. Determination of this difference is important since any advantage or disadvantage of CLC vs. conventional combustion technology influences the attractiveness for commercialization of biomass CLC. There are two key differences between CLC of biomass and conventional fluidized bed biomass boilers:

1. Fuel oxidation mechanism: biomass is oxidized in air in a conventional fluidized bed boiler, while in CLC, biomass is oxidized by the oxygen carrier bed material
2. Bed materials: conventional biomass fluidized bed boilers use silica sand bed material, while in CLC, the oxygen carrier is the bed material

The current study focused on determining how the fuel oxidation difference between CLC and conventional fluidized bed combustion influences fuel alkali release. As such, CLC operation of the pilot reactor was tested against oxygen carrier aided combustion (OCAC) [23]. The OCAC mode of operation is essentially a conventional fluidized bed combustion process operated with an oxygen carrier, instead of silica sand. In OCAC, like in conventional fluidized bed biomass boilers, the majority of the fuel is oxidized by air that is used to fluidize the fuel reactor. Testing CLC operation vs. OCAC operation allows to determine the effect of the fuel oxidation mechanism (oxidation by air in OCAC vs. oxidation by oxygen carrier is CLC), while keeping the bed material and the associated alkali interaction effects constant.

## 3. Experimental setup

The following subsections summarize the experimental setup used in this experimental study.

### 3.1. Pilot reactor system

Experimental tests in this study were conducted in a dual circulating fluidized bed (D-CFB) process development unit (PDU) located at VTT Bioruukki piloting center in Espoo, Finland. As setup for chemical looping operation, this system consists of two interconnected circulating fluidized beds, one serving as the air reactor (AR) and the other as the fuel reactor (FR), as illustrated in Fig. 1. The nominal fuel power of the reactor system in CLC operation is 60 $kW_{th}$.

Each of the two CFB units consist of a riser, an outlet cyclone for solids separation, and a solids return leg that is used to interconnect the reactors. The AR has a height of 6425 mm, an internal diameter of 150 mm, and is setup to be fluidized with air. The FR consists of two sections: the lower section with a height of 2070 mm and an internal diameter of 100 mm, and the upper section with a height of 6290 mm and an internal diameter of 150 mm. The FR can be fluidized with air, nitrogen, or superheated steam. Each of the two reactors is equipped with a solids feeding system capable of feeding make-up bed material and solid fuels. Each reactor is electrically heated and insulated to facilitate warm-up of the system, as well as to control process temperature during experiments. Fly ash removal from the AR flue gas is handled by a baghouse filter system. For the FR, the fly ash is removed by a high efficiency cyclone.

Process variables for process control and monitoring (flow rates, temperatures, pressures) are controlled and logged in a central control and data acquisition system. The D-CFB system is also equipped with gas sampling. AR flue gas is sampled downstream of the baghouse filter, while the FR flue gas is sampled downstream of the high-efficiency cyclone. Each of the two flue gas streams are analysed for $O_2$, $CO_2$, CO, $H_2$, $CH_4$ by on-line gas analysers (ABB AO2020). Flue gas alkali sampling is implemented just downstream of the cyclones of both reactors. A detailed description of the alkali sampling system is provided in Section 3.3.

### 3.2. Oxygen carriers and fuels

Two oxygen carriers were tested in this experimental campaign, ilmenite and braunite. Norwegian ilmenite with a purity of >95% $TiFeO_3$ and a mean particle size of ($d_{50}$) of 270 μm was supplied by Titania A/S, Norway. Ilmenite is the most widely tested oxygen carrier in CLC of solid fuels as it combines reasonable reactivity, high resistance to attrition, and relatively low cost. For CLC of biomass, ilmenite is potentially especially suitable as it is known to absorb alkalis through formation of alkali titanates [24,25]. Additionally, the only alkali emissions measurements in CLC of biomass published to date were collected in CLC tests with pure ilmenite [7] and a mixed ilmenite/calcium manganite oxygen carrier [8]. Thus, ilmenite is a good basis for comparison of alkali emissions of this system to previously published results.

Swedish braunite, supplied by Sibelco Nordic AB, Sweden, is a manganese-silicate ore with a general formula of $Mn_7SiO_{12}$. This material consists of >70 wt% $Mn_2O_3$ and $Mn_3O_4$ and has a mean particle diameter of 234 μm. Braunite was selected since manganese ores are generally more reactive than ilmenite and may also enable partial chemical looping with oxygen uncoupling (CLOU) operation. The CLOU effect refers to CLC operation with oxygen carriers that release some free oxygen in the reducing atmosphere of the FR. CLOU carriers thus enhance fuel conversion by enabling partial direct fuel oxidation in addition to the gas–solid reaction of a non-CLOU oxygen carrier. From the alkali release perspective, braunite does not contain significant levels of titanium, and thus was not expected to absorb alkalis in the

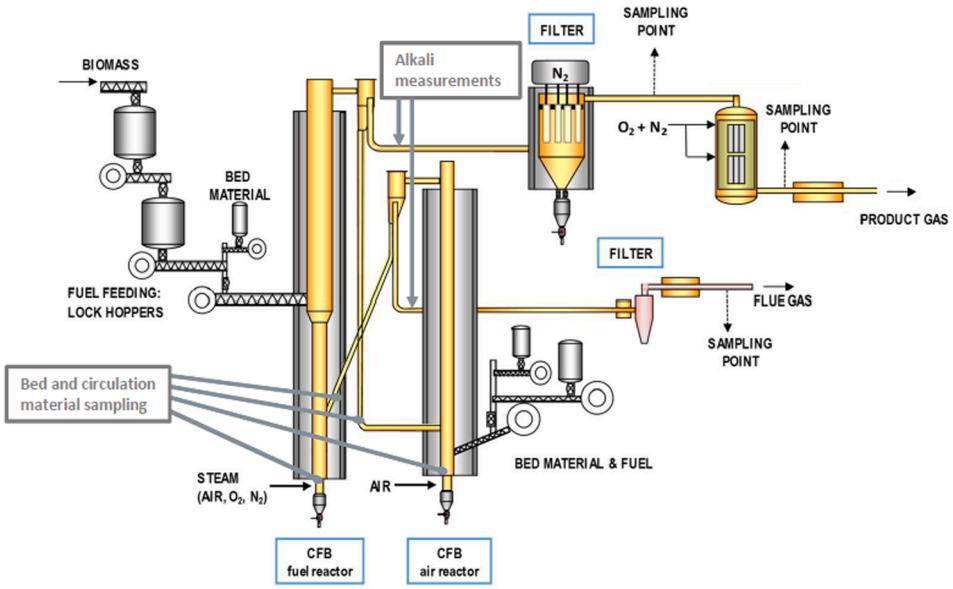


**Fig. 1.** Schematic of the dual circulating fluidized bed chemical looping combustion pilot.

same manner as ilmenite. The elemental composition of the two oxygen carriers used in this study is presented in Table 1.

The fuels used for the campaign were selected to range in their volatiles content and in their alkali content. The composition of the tested fuels and their key properties are presented in Table 2. Wood pellets (WP) and straw pellets (SP) are biomass fuels have a volatiles content >69 wt%, whereas wood char (WC) has a low volatiles content of only 18.7 wt%. Since a fuel's volatile fraction affects the fuel decomposition and conversion process, testing fuels of low and high volatiles fractions was carried out to observe if and how volatiles content affects the alkali release process. The experimental fuels were also selected to vary in their alkali content. Wood pellets (WP) fuel has an alkali content that is typical of biomass fuels used in conventional biomass boilers. Straw pellets (SP) fuel, on the other hand, has a very high alkali and chlorine content. This fuel represents a biomass that would be challenging to use in conventional biomass boilers without implementing measures to limit gas phase alkali release, such as co-firing with sulphur-containing fuels, or using sulphur addition. Wood char (WC) fuel has a relatively high alkali content but does not have a high chlorine content. Fuels with a wide range of alkali and chlorine content were used to observe how fuel composition differences can affect alkali release dynamics.

**Table 1**
Oxygen carrier elemental composition.

| Element | Unit | Ilmenite | Braunite |
|---|---|---|---|
| Ti | wt % | 27.36 | 0.020 |
| P | wt % | 0.004 | 0.030 |
| S | wt % | 0.026 | 0.13 |
| Cr | wt % | 0.051 | 0.010 |
| Fe | wt % | 35.89 | 11.0 |
| Si | wt % | 0.76 | 2.50 |
| V | wt % | 0.11 | <0.01 |
| Ca | wt % | 0.15 | 3.50 |
| Mg | wt % | 2.23 | 0.89 |
| Al | wt % | 0.34 | 0.25 |
| Mn | wt % | 0.23 | 55.0 |
| K | wt % | 0.017 | 0.020 |
| Na | wt % | 0.052 | 0.22 |
| Zn | wt % | 0.012 | 0.010 |
| Ni | wt % | 0.018 | 0.010 |
| Cu | wt % | 0.007 | 0.040 |
| Co | wt % | 0.012 | 0.020 |
| Sr | wt % | 0.003 | 0.12 |
| Zr | wt % | 0.017 | 0.020 |
| Nb | wt % | 0.005 | <0.0001 |
| Pb | wt % | <0.0001 | 0.010 |
| Cl | wt % | <0.01 | 0.030 |
| O (remainder) | wt % | 32.7 | 26.2 |

### 3.3. Alkali measurement system

An online alkali measurement technique based on the principle of surface ionization detection (SID) was implemented in this experimental campaign. A detailed overview of the SID principle is available in reference [26], and its implementation for online alkali measurement is captured in reference [27,28] for bench-scale investigations, and in references [8,20,29] for industrial and pilot scale investigations. A brief overview of the system is provided for completeness. Fig. 2 shows a schematic of the system as implemented in this study.

The SID alkali measurement system shown in Fig. 2 was setup for measurement of alkali emissions in the AR and FR flue gases. However, only one reactor, either the AR or FR, could be sampled at a time. The sample suction and conditioning systems were essentially replicated on the AR and the FR, allowing the SID instrumentation to be switched between the two reactors through valve manipulation. When sampling, flue gas is drawn at the process temperature (750–950 °C) by a specially designed probe and is then diluted by nitrogen in three serial stages. First dilution occurs inside the sampling probe as soon as the sample gas enters the probe. The second stage of dilution is carried out in a wall-flow diluter installed immediately after the exit of the sample probe. The third stage of dilution is carried out in a Dekati diluter installed on the SID instrument rack, just upstream of the diluted sample distribution manifold. The Dekati diluter operates as a venturi device, thus creating the suction used to draw the flue gas sample from the process. The nitrogen flow supplied to the three dilution stages is carefully controlled by electronic mass flow controllers. Dilution is carried out to quench the sample such that liquid and gaseous alkali salt species condense into solid aerosol particles that are less prone to deposition on the sampling system's internal surfaces. Dilution is also needed to make the sampled gas easier to handle to and to avoid condensation of steam that may be present in the sample. The targeted overall dilution ratio is in the range of 50 to 200. However, probe contamination and process pressure variation ultimately result in a constantly changing dilution ratio which needs to be closely monitored.

After three stages of dilution, the diluted sample leaves the Dekati diluter at approximately 25 °C and is distributed via a manifold to the

**Table 2**
Biomass fuel properties.

| Parameter | Unit | Wood Pellets (WP) | Wood Char (WC) | Straw Pellets (SP) |
|---|---|---|---|---|
| Moisture | wt % a.r. | 7.50 | 4.10 | 8.10 |
| Ash | wt % a.r. | 0.460 | 14.0 | 5.51 |
| Volatiles | wt % a.r. | 78.4 | 18.7 | 69.3 |
| Fixed Carbon | wt % a.r. | 13.7 | 63.2 | 17.1 |
| H | wt % a.r. | 5.64 | 2.21 | 5.24 |
| C | wt % a.r. | 46.9 | 73.0 | 43.2 |
| N | wt % a.r. | 0.160 | 0.960 | 0.580 |
| O | wt % a.r. | 39.4 | 5.75 | 37.2 |
| K | mg/kg fuel a.r. | 202 | 1560 | 6870 |
| Na | mg/kg fuel a.r. | 122 | 114 | 61.0 |
| Cl | mg/kg fuel a.r. | 26.0 | 101 | 3320 |
| S | mg/kg fuel a.r. | 93.0 | 288 | 1010 |
| Si | mg/kg fuel a.r. | 88.0 | 378 | 9210 |
| Ca | mg/kg fuel a.r. | 994 | 47,000 | 3360 |
| LHV | MJ/kg a.r. | 17.3 | 26.1 | 15.8 |
| Bulk Density | kg/m3 a.r. | 476 | 368 | 332 |
| Particle Size Range | mm | 2–6 | 3–8 | 2–6 |
| K/Cl Molar Ratio | mol/mol | 6.93 | 14.0 | 1.88 |
| K/Si Molar Ratio | mol/mol | 1.64 | 2.96 | 0.540 |

SID instrument rack consisting of the SID detector, a $CO_2$ analyser, a trace $O_2$ analyser, and a scanning mobility particle sizer (SMPS). The SID detector measures the diluted sample's alkali concentration. To recalculate SID alkali measurements back to process conditions, time-resolved monitoring of the sample dilution ratio is critical. When sampling the FR, the sample's overall dilution is tracked using $CO_2$ as a tracer gas. The raw FR flue gas concentration is measured by the main process gas analysers, while the diluted sample $CO_2$ concentration is measured by an independent $CO_2$ analyser (LICOR LI-850) installed on the SID instrument rack. Dividing the raw flue gas $CO_2$ concentration by the diluted sample's $CO_2$ concentration gives the overall sample dilution ratio. Similarly, the AR dilution is tracked using $O_2$ as a tracer gas. The raw flue gas oxygen concentration is measured by the main process gas analyser, while the diluted sample's $O_2$ concentration is measured by the trace-$O_2$ analyser (Alpha Omega Instruments 3000-Y230BTP), installed on the SID instrument rack. The sample's overall dilution ratio is calculated by diving the raw AR flue gas $O_2$ concentration by the diluted sample's $O_2$ concentration.

The SMPS system (TSI SMPS 3082 & CPC 3750) is primarily used for calibration of the SID. During calibration a polydisperse aerosol generator (TSI 3073) with a 0.005 M $KCl_{(aq)}$ solution is used to generate a stream of fine aqueous KCl aerosol droplets suspended in air. This stream is then passed through a diffusion dryer, resulting in precipitation of solid $KCl_{(s)}$ particles. The resulting $KCl_{(s)}$ aerosol stream is split and routed to the SMPS and the SID instruments. The SMPS is used to measure the aerosol's mass concentration, while the SID measures the alkali concentration by surface ionization detection. Varying the aerosol generator's settings allows for generation of aerosol streams of varying mass concentration. Plotting the linear response of the SID vs. the aerosol concentration measured by the SMPS gives a linear calibration plot of the SID response. This calibration is then used to translate the SID signal to alkali concentration measurements during process measurements. In the three days of this campaign, the SID instrument was calibrated twice. Deviation between the calibrations indicated that the SID response had an approximate measurement drift of + 1.5% per hour of operation. This drift value is consistent with this instrument's performance in a different measurement campaign [7]. This drift value is the best estimate of the instrument error and was deemed acceptable for

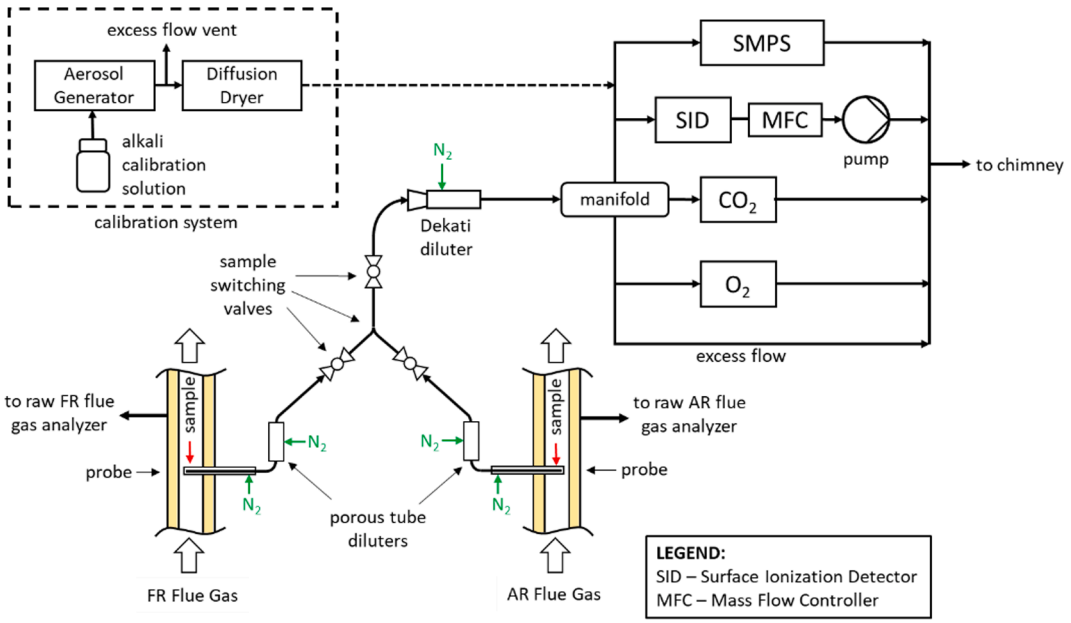


**Fig. 2.** SID online alkali measurement system simplified schematic.

relative comparison of the results. It should be noted that further to the SID instrument error, the error associated with sampling losses (losses due to deposition of alkali aerosol on the inner walls of the sampling equipment) represents an unknown but likely a significant source of alkali measurement uncertainty. Sampling losses are common to all extractive techniques, and the SID sampling system was designed to minimize sampling losses by implementing best practices in aerosol sampling. Since some sampling losses are still expected to occur, the SID alkali concentrations reported in the results likely underestimate the measured alkali concentrations. Nevertheless, in the authors' opinion, the SID technique represents the best available online alkali measurement technique available for pilot investigations. Moreover, alkali mass balance of bed material in previous pilot measurements gave strong support for SID measurements, only finding a minor fraction of alkalis in the exit gases[8].

### 3.4. Calculation of carbon capture efficiency

Oxide oxygen efficiency is a measure of carbon capture efficiency and is defined as the ratio of the oxygen used for oxidation of the OC in the AR to the total oxygen consumed in the AR:

$$\eta_{oo}[\%] = 100*\frac{0.2099 - (1+d)x_{O2,AR} - (1+d)x_{CO2,AR}}{0.2095 - (0.9996+d)x_{O2,AR} - 0.2095x_{CO2,AR}} \quad (1)$$

$$\text{Were } d = \frac{\dot{Q}_{dilutionN2}}{\dot{Q}_{air}} \quad (1.1)$$

Here $d$ is the ratio of the AR dilution nitrogen to the AR air flow. AR dilution nitrogen is comprised of various nitrogen purge streams (i.e. pressure tap purge nitrogen, cyclone return leg L-valve purge nitrogen). Coefficients in Eq. (1) also account for the fact that air fed to the AR contains 400 ppm of $CO_2$. The calculation shown in Eq. (1) is based on the fact that $CO_2$ detected in the AR is caused by combustion of unconverted fuel carried-over from the FR to the AR. Thus, deviation from 100% carbon capture efficiency is indicative of fuel carryover to the AR.

### 3.5. Experimental plan

Experiments using the D-CFB CLC system were conducted over a duration of three days. Ilmenite was tested with wood pellets (WP) and wood char (WC), while braunite was tested with wood pellets (WP), wood char (WC), and straw pellets (SP). A total of seven CLC tests were performed. Prior to starting CLC tests, the dual circulating fluidized bed system had to be warmed up to typical CLC temperatures of approximately 900 °C. The electric heaters installed on the reactor system were underpowered, so additional preheating was achieved by running both reactors as combustors. The pilot system was started with air fluidizing both reactors, and once electrical heaters raised the reactor temperature to approximately 600 °C, biomass fuel was fed to the AR and FR reactors, initiating combustion. Fluidized bed combustion in presence of an oxygen carrier is known as oxygen carrier aided combustion (OCAC)[23]. In OCAC, the oxygen carrier helps in buffering oxygen distribution in the bed. However, in terms of fuel conversion, OCAC is most like a conventional fluidized bed combustion process, where most of the fuel is oxidized with air. The OCAC operation of the pilot system helped warm up the reactor system past the capability of the electric heaters. Once the system reached approximately 900 °C, CLC tests were started by stopping the fuel feed to the AR and switching FR fluidization to steam. The OCAC pre-heating periods prior to the start of CLC tests presented a unique opportunity to measure alkali emissions in two distinct combustion modes.

## 4. Results and discussion

Alkali emissions were measured with the SID system throughout the

**Table 3**
Average alkali emissions measured with the SID instrument.

| Test | OC | OC Inventory | Test Mode | Duration | Period | Fuel Reactor | | | | | | Air Reactor | | | | | |
|---|---|---|---|---|---|---|---|---|---|---|---|---|---|---|---|---|---|
| | | | | | | FR Fuel | FR Fuel Feed Rate (g/s) | FR Alkali Feed (mg $K_{eq}$/min) | FR Avg Alkali Emissions (mg $K_{eq}$/min) | % of Incoming Alkalis Released | Average Bed Temperature (°C) | AR Fuel | AR Fuel Feed Rate (g/s) | AR Alkali Feed (mg $K_{eq}$/min) | AR Avg Alkali Emissions (mg $K_{eq}$/min) | % of Incoming Alkalis Released | Average Bed Temperature (°C) |
| Test_1 | Ilmenite | 59 kg | OCAC | 00:51 | 1 | WP | 1.9 | 36.8 | 0.22 | 0.59% | 887 | WP | 1.3 | 25.1 | – | – | 889 |
| | | | CLC | 01:13 | 2 | | 1.9 | 36.8 | 0.69 | 1.88% | 786 | | – | – | 0.24 | – | 826 |
| Test_2 | Ilmenite | 59 kg | OCAC | 00:22 | 3 | WP | 1.9 | 36.8 | 0.32 | 0.86% | 907 | WP | 1.9 | 36.8 | – | – | 911 |
| | | | CLC* | 00:39 | 4 | | 2.5 | 48.5 | 0.74 | 1.53% | 805 | | 0.7 | 13.4 | 0.20 | 1.48% | 874 |
| Test_3 | Ilmenite | 58 kg | OCAC | 00:50 | 5 | WC | 1.2 | 118.5 | 0.19 | 0.16% | 898 | WP | 1.9 | 36.8 | – | – | 911 |
| | | | | | 6 | | 1.9 | 192.8 | 0.19 | 0.10% | 916 | | 1.9 | 36.8 | – | – | 921 |
| | | | | | 7 | | 2.4 | 239.3 | 0.34 | 0.14% | 930 | | 1.9 | 36.8 | 0.27 | 0.73% | 914 |
| | | | CLC | 01:25 | 8 | | 2.4 | 239.3 | 3.78 | 1.58% | 794 | | – | – | – | – | 851 |
| Test_4 | Ilmenite | 57 kg | CLC | 00:39 | 9 | WC | 3.3 | 332.3 | 4.42 | 1.33% | 821 | WP | – | – | 0.30 | – | 859 |
| Test_5 | Braunite | 66 kg | OCAC | 00:59 | 10 | WP | 2.7 | 53.1 | 1.50 | 2.83% | 901 | WP | 1.9 | 36.8 | 1.25 | 3.40% | 910 |
| | | | CLC | 02:51 | 11 | | 3.7 | 71.8 | 2.49 | 3.47% | 828 | | – | – | 0.77 | – | 873 |
| | | | | | 12 | | 4.3 | 83.5 | 1.89 | 2.27% | 824 | | – | – | 0.70 | – | 885 |
| | | | | | 13 | | 2.5 | 48.5 | 1.12 | 2.30% | 830 | | – | – | – | – | 859 |
| Test_6 | Braunite | 63 kg | OCAC | 00:18 | 14 | WC | 1.5 | 146.3 | 0.28 | 0.19% | 896 | WP | 1.9 | 36.8 | – | – | 885 |
| | | | CLC | 00:56 | 15 | | 2.8 | 285.8 | 3.66 | 1.28% | 816 | | – | – | 1.44 | – | 903 |
| Test_7 | Braunite | 63 kg | OCAC | 01:03 | 16 | SP | 2.6 | 1073.8 | 2.99 | 0.28% | 889 | WP | 1.9 | 36.8 | – | – | 892 |
| | | | CLC | 01:58 | 17 | | 3.0 | 1248.4 | 54.66 | 4.38% | 810 | | – | – | 35.00 | – | 857 |

* Partial CLC operation with fuel fed to the AR as well as FR

duration of the experimental campaign. Alkali concentration data reported in this section has been processed to omit erroneous alkali measurements that occur during major sampling operation disturbances. Such disturbances include periods for alkali sample probe backflushing and transients associated with switching the alkali sampling system between the two reactors. A summary of averaged release rates for all campaign test is presented in Table 3. In interpreting the presented results it is important to recognize that the SID selectively measures alkali species that contain K and Na [28]. However, the measured response of the SID cannot differentiate whether the signal is a result of Na-containing alkali species or K-containing alkali species. Since K is the dominant alkali cation in biomass, alkali measurement results are reported as mg of potassium equivalents ($K_{eq}$).

Table 3 reports results for the OCAC and CLC tests, listed by the oxygen carrier and fuel used. In some cases, CLC and OCAC tests have been subdivided by different fuel feeding rates into periods. The periods are numbered sequentially (1 through 17) and will be used to facilitate discussion. Figs. 3 through 6 show alkali emissions plots for several tests.

### 4.1. Alkali emissions variability

Alkali emissions data presented in Figs. 3 through 7 exhibits significant in-test variability for CLC operation. Although steady CLC operation of the D-CFB pilot was targeted, major challenges were encountered in maintaining steady temperatures and balanced oxygen carrier inventories in the AR and the FR. In order to give an impression of the variability of different test parameters in relation to alkali measurements, Figs. 7 through 9 show the alkali emissions and key operating parameters for Test 5 conducted with braunite oxygen carrier and wood pellets fuel.

Fig. 8 shows that both the FR and AR bed temperatures generally decreased with a switch to CLC operation. This was the case for all of the conducted CLC tests. Aside from the general decrease trend, the bed temperatures in almost all tests exhibited variation. An example of such variation is shown in Fig. 8. There, the two low points of the AR bed temperature coincide with FR fuel feeding interruptions shown in Fig. 7. The reasons for the residual fluctuations are unclear but are possibly related to instability in the circulation of the bed material between the two reactors. Unstable circulation was suspected for all the conducted CLC tests as significant AR and FR bed pressure drop fluctuations indicated a transfer of inventory between the two reactors. An example of such fluctuations can be seen in Fig. 8 for Test 7. Variability was also seen in the FR gas concentrations and carbon capture efficiency, as shown for Test 7 in Fig. 9. Variation of the FR gas concentrations is indicative of varying fuel conversion or an unstable fuel feeding rate. Changes in carbon capture efficiency are indicative of changes in carryover of unconverted fuel to the AR.

In reviewing the variation of operating conditions for all of the conducted tests, correlations of the measured alkali concentrations to a number of operational parameters could be identified. As an example, the change in FR alkali concentration for CLC operation in Tests 1, 4, and 5 correlated with FR bed temperature, as well as with FR $CO_2$ concentration and FR bed pressure drop. However, FR alkali concentration showed a negative correlation with FR bed temperature, no correlation with FR pressure drop, and positive correlation with AR bed temperature in Tests 3 and 7. Looking at the different processes that control alkali release and retention, several of these correlations make sense. However, the relation between process conditions and alkali emissions is quite complex. When comparing the different tests, it is not possible to pinpoint any individual parameter that can consistently explain the variations in the measured alkali concentrations. In conclusion, analysis of the operational parameters indicated that the CLC D-CFB pilot exhibited only semi-stable operation, and it is likely that variability of multiple operating parameters explains the variability of alkali emissions measurements to a significant extent.

### 4.2. CLC vs. OCAC gas-phase alkali emissions

In light of the variation in the D-CFB pilot's operating parameters, a significant effort to minimize data error was made in compiling the average emissions results presented in Table 3. Data averaging periods in Table 3 were selected to omit transient operation associated with test start-up periods as well as periods of operational disturbances (e.g. short-term fuel feeding stops to refill the fuel hopper). As such, the average data presented in Table 3 is deemed adequate for high level comparison of alkali emissions levels between different tests.

Review of the results presented in Table 3 suggests a few trends. The first is that for the ilmenite tests, alkali release levels in the FR seem to be higher in CLC operation vs. OCAC operation. This is evident in comparing periods 1 and 2 (Test 1) for operation with wood pellets, and periods 7 and 8 (Test 3) for operation with wood char. In both cases, the FR is operated at a steady fuel feeding rate, but as operation is switched from OCAC (for pre-heating) to CLC mode, FR alkali emissions increase by a factor of 3 for wood pellets operation, and by a factor of 11 for operation with wood char. Figs. 3 and 4 clearly show these transitions. The onset of CLC operation clearly coincides with the escalation of FR alkali emissions.

For tests conducted with braunite, this escalation of FR emissions is more difficult to assess since the FR fuel feed rates differ for the OCAC and CLC tests. Comparison of FR alkali emissions requires the assumption that alkali release in the FR should be proportional to the fuel feed rate. Assuming this, for operation with braunite and wood pellets (Test

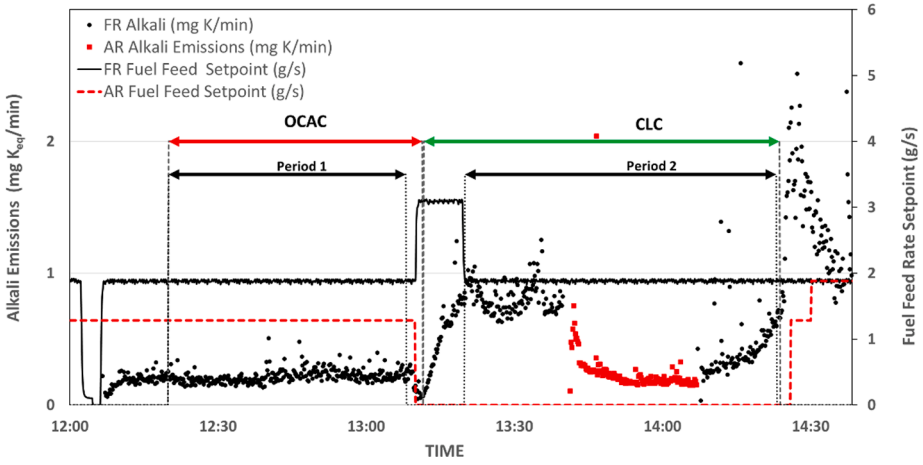


**Fig. 3.** Alkali emissions for Test 1 (ilmenite & wood pellets).

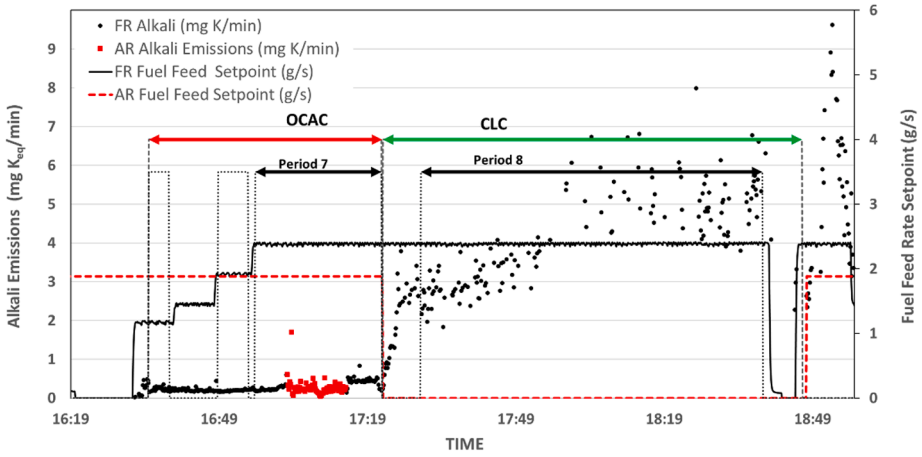


**Fig. 4.** Alkali emissions for Test 3 (ilmenite & wood char).

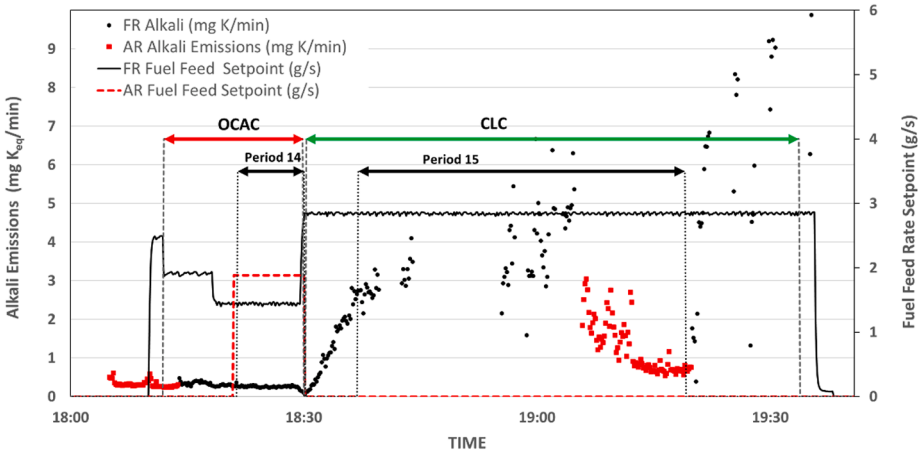


**Fig. 5.** Alkali emissions for Test 6 (braunite & wood char).

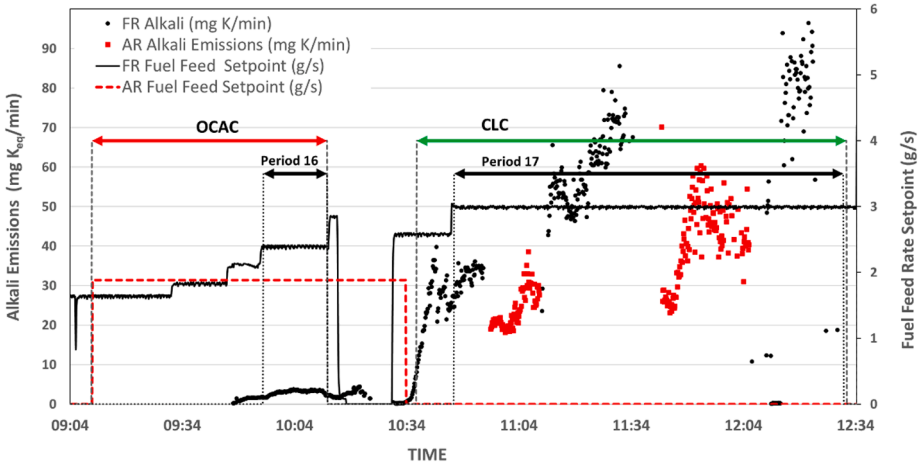


**Fig. 6.** Alkali emissions for Test 7 (braunite & straw pellets).

5), FR alkali emissions are roughly equivalent in OCAC and CLC modes (see Fig. 7). However, for operation with wood char (Test 6) and straw pellet fuels (Test 7), FR emissions in CLC mode are substantially higher than in OCAC. In fact, the escalation of alkali emissions that comes with transition to CLC, increases with higher fuel alkali content; FR alkali emissions increase approximately by a factor of 7 for wood char and by approximately by a factor of 15 for straw pellets. Figs. 5 and 6 show the escalation of FR alkali emissions at the onset of CLC operation for Tests 6 and 7.

Considering the observed escalation trend, FR bed temperatures between OCAC and CLC operation were reviewed. Table 3 indicates that average FR bed temperatures in CLC tests are 70 °C to 140 °C lower

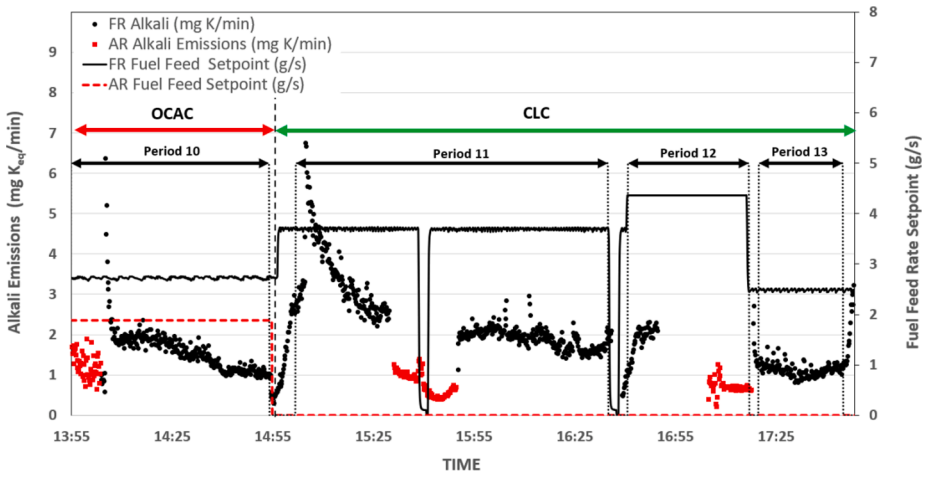


**Fig. 7.** Alkali emissions for Test 5 (braunite & wood pellets).

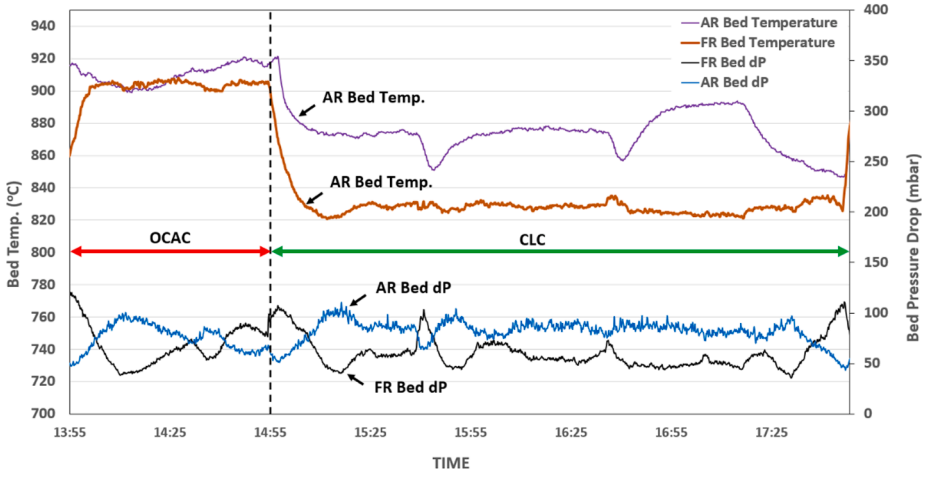


**Fig. 8.** Reactor bed temperatures and pressure drops for Test 5 (braunite & wood pellets).

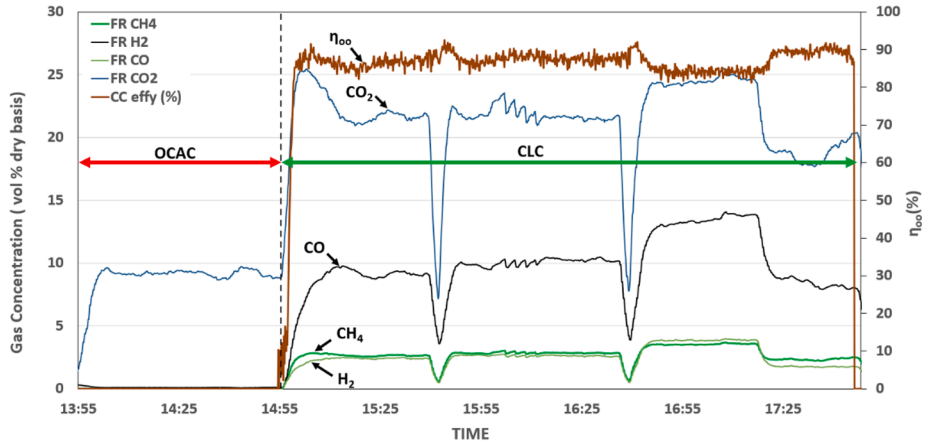


**Fig. 9.** FR gas concentrations and carbon capture efficiency for Test 5 (braunite & wood pellets).

when compared to preceding OCAC tests. Alkali release in fuel conversion processes is known to be proportional to temperature [30,31]. Thus, the bed temperature difference between CLC and OCAC modes cannot explain the higher FR alkali emissions in CLC.

### 4.3. Alkali release during fuel conversion

Difference in the gas composition and the fuel decomposition processes in OCAC and CLC operation were considered as potential factors in the observed alkali emissions trend. In OCAC, the gas composition in the FR is oxidizing, mostly consisting of $N_2$, trace amounts of $CO_2$ and up

to 10 vol% $O_2$. As the switch to CLC operation is made, FR fluidization is switched from air to steam with product gases consisting primarily of $H_20$, $CO_2$, and minor amounts of $N_2$, $H_2$, and CO. Gaseous $O_2$ is no longer present as all oxygen for fuel conversion is now sourced from the oxygen carrier. The significantly different atmosphere of the two combustion modes may influence two of the main competing processes that control the net alkali release to the flue gas. These are:

1) Alkali release to the gas phase - the process by which alkalis are released from the fuel's matrix to the gas phase
2) Alkali retention in the bed - the processes by which the released alkalis are trapped in the bottom ash or in the bed material

In determining how the reactor atmosphere can influence alkali release from the fuel, the fuel decomposition process needs to be considered. In the OCAC, which is a process of fuel combustion in air, the first stage as the fuel enters the reactor is devolatilization. In devolatilization, volatile components rapidly evaporate from the fuel's matrix. Since the fuel particles used in this study are quite small (2–8 mm), this process is fast with a large outward flux of volatile components leaving the fuel particle. This is especially true for the wood pellets and straw pellets fuels, as their volatiles fraction is higher than 69%. Because of this outward flux, external gaseous species in the fuel reactor's atmosphere cannot penetrate the fuel particle and are unlikely to influence the devolatilization process. For this reason, the devolatilization stage should be identical in OCAC and CLC cases. Studies measuring release of K in devolatilization of biomass estimate that < 10 wt% of the fuel's total K content is released in the devolatilization stage at temperatures below 700 °C, where organically associated K is released as KOH(g) or as part of the tar fraction [31,32]. Thus, for a given fuel, the release of K that occurs during devolatilization should be quite low and approximately equivalent in CLC and OCAC modes.

By the stage where the fuel particle is heated beyond 700 °C, devolatilization is mostly complete, with the solid char fraction remaining. As K release in devolatilization is minimal, most of the fuel's K remains in the char in the form of alkali salts or in silicate form. In the OCAC case, devolatilization is followed by char burnout. As the char temperature exceeds 700 °C, KCl vapor pressure rises, and evaporation of KCl to the gas phase becomes the most significant release pathway of K release. This path, however, is limited by Cl availability and formation of potassium silicates. Cl availability depends on the fuel's original Cl content and the amount of Cl that is released in the devolatilization stage. Cl release in devolatilization can reach up to 60%, depending on the fuel [10,31,33]. Formation of non-volatile potassium silicates and aluminosilicates competes for K and becomes more significant as the char temperature rises during char burnout. Further to KCl sublimation, high temperature dissociation of carbonates and sulfates, which becomes significant at temperatures approaching 900 °C, contributes to further K release [32].

In CLC, char that remains after devolatilization undergoes gasification with steam, followed by the reaction of the volatiles and gasification products with the oxygen carrier [14]. K release during the gasification stage of CLC has not been previously studied. However, the conditions of the gasification step in CLC are similar to those in conventional steam gasification: high temperature (800–1000 °C), no free oxygen, excess steam. In conventional steam gasification, release of K through evaporation of KCl to the gas phase is also the predominant mechanism, although the presence of steam tends to reform some of the KCl(g) to KOH(g) and HCl(g)[34]. In the CLC gasification step, conditions are similar, and the net K release from the char through KCl evaporation (released as KCl(g), or reformed by steam to KOH(g), is expected to be similar to conventional steam gasification and combustion and thus cannot explain the higher observed release of K to the flue gas.

A possible explanation for higher alkali release in CLC is that K release originating from $K_2CO_3$ and $K_2SO_4$ salts that remain in the char fraction after the devolatilization occur differently in OCAC and CLC. Novakovic et al. studied the K release in K-Ca-Si system with controlled release experiments. Their experiments showed that the presence of water vapor greatly enhanced the rate of high temperature decomposition of $K_2CO_3$. This effect was attributed to $K_2CO_3$ reacting with steam to form KOH(g) [35]. Similarly, a study on interaction of ilmenite with $K_2CO_3$ and $K_2SO_4$, showed that presence of steam in the reacting atmosphere enhanced the release of K to the gas phase through formation of KOH(g) [36]. For the fuels used in the current study, the molar ratios of K to Cl are 6.93 for the wood pellets fuel, 14.01 for the wood char fuel, and 1.88 for the straw pellets fuel. Assuming that for the two high-volatiles fuels (wood pellets and straw pellets) a significant portion of the Cl is released in the devolatilization stage, indicates that the K to Cl ratios in the remaining char fraction are even higher, and that a significant portion of the fuel's K can be present in the form of $K_2CO_3$ and $K_2SO_4$ salts. Therefore, the steam fluidizing medium in the CLC process likely accelerates the decomposition of $K_2CO_3$ and $K_2SO_4$ salts, resulting in a significant gaseous release of K as KOH(g).

### 4.4. Alkali retention

In order to gain a more complete understanding of the alkali behavior, the processes governing the retention of alkalis in condensed phases are also important to consider. Table 4 presents a mass balance of the alkalis in the system. Here, alkali retention is estimated by subtracting the measured gas-phase alkalis release from the alkalis introduced into the reactor with the fuel.

The mass balance in Table 4 shows that from the total alkali input into the system, most of the alkalis are retained in a condensed phase. Tests conducted with ilmenite show a retention >97%, while tests with braunite show a retention >92% for all fuels used. The results for ilmenite are consistent with alkali retention estimates presented for investigations with ilmenite [7] and ilmenite and calcium manganite mixed OC [8]. Retention of alkalis in the condensed phase can occur through several processes:

1) Alkali retention by formation of fuel ash
2) Alkali retention by the OC material
3) Alkali retention by deposition on reactor walls

The first path accounts for alkalis that are retained by formation of ash that originates from the fuel itself. In this case, fuel alkalis are trapped in the ash fraction through formation of alkali silicates, as well as other stable species. Experiments quantifying potassium release of annual biomass at conditions resembling grate-fired furnaces show that at combustion temperatures of 800–900 °C, <20% of K is released in combustion of low-Cl biomass, and < 40% of K is released in combustion of high-Cl annual biomass [32]. Similar experiments for different types of woody biomass report similar rates in the range of 20–40% of K in the temperature range of 800–900 °C [37]. Since grate-fired furnace conditions imply no extraneous material and long fuel residence times, these release rates approximate the maximum alkali gas-phase release from biomass that can be expected to occur with no influence of extraneous material, such as an oxygen carrier. Thus, in a combustion process, approximately up to 60–80% of fuel alkalis can be retained through fuel ash formation alone. In CLC, alkali retention by ash formation, excluding any effects of the OC material, should be somewhat lower. This is due to the aforementioned effect that steam has on accelerating the decomposition of $K_2CO_3$ and $K_2SO_4$ in CLC operation. It should be noted that a significant portion of fuel ash is likely to be elutriated from the reactor system as fly ash.

The second pathway for retention of alkali in CLC, is the retention due to interaction of alkalis with the OC material. Several bed material samples were collected during the campaign and analyzed for elemental composition. For ilmenite, only one sample was taken after 50 min of CLC operation with wood pellets fuel. Due to the short operation time and the low alkali content of wood pellets, the exposure of ilmenite to

**Table 4**
System alkali balance.

| | | | | | Total System Balance | | | |
|---|---|---|---|---|---|---|---|---|
| **Test** | **OC** | **Test Mode** | **Period** | **FR Fuel** | **System Total Alkali Feed (mg $K_{eq}$ /min)** | **% Alkali in FR Flue Gas** | **% Alkali in AR Flue Gas** | **% Retention** |
| **Test_1** | **Ilmenite** | **OCAC** | **1** | **WP** | 61.9 | 0.35% | – | – |
| | | **CLC** | **2** | | 36.8 | 1.88% | 0.65% | 97.47% |
| **Test_2** | **Ilmenite** | **OCAC** | **3** | **WP** | 73.6 | 0.43% | – | – |
| | | **CLC*** | **4** | | 61.9 | 1.20% | 0.32% | 98.48% |
| **Test_3** | **Ilmenite** | **OCAC** | **5** | **WC** | 155.2 | 0.12% | – | – |
| | | | **6** | | 229.6 | 0.08% | – | – |
| | | | **7** | | 276.1 | 0.12% | 0.10% | 99.78% |
| | | **CLC** | **8** | | 239.3 | 1.58% | – | – |
| **Test_4** | **Ilmenite** | **CLC** | **9** | **WC** | 332.3 | 1.33% | 0.09% | 98.58% |
| **Test_5** | **Braunite** | **OCAC** | **10** | **WP** | 89.9 | 1.67% | 1.39% | – |
| | | **CLC** | **11** | | 71.8 | 3.47% | 1.07% | 95.46% |
| | | | **12** | | 83.5 | 2.27% | 0.84% | 96.90% |
| | | | **13** | | 48.5 | 2.30% | – | – |
| **Test_6** | **Braunite** | **OCAC** | **14** | **WC** | 183.1 | 0.15% | – | – |
| | | **CLC** | **15** | | 285.8 | 1.28% | 0.50% | 98.22% |
| **Test_7** | **Braunite** | **OCAC** | **16** | **SP** | 1110.5 | 0.27% | – | – |
| | | **CLC** | **17** | | 1248.4 | 4.38% | 2.80% | 92.82% |

*Partial CLC operation with fuel fed to the AR as well as FR

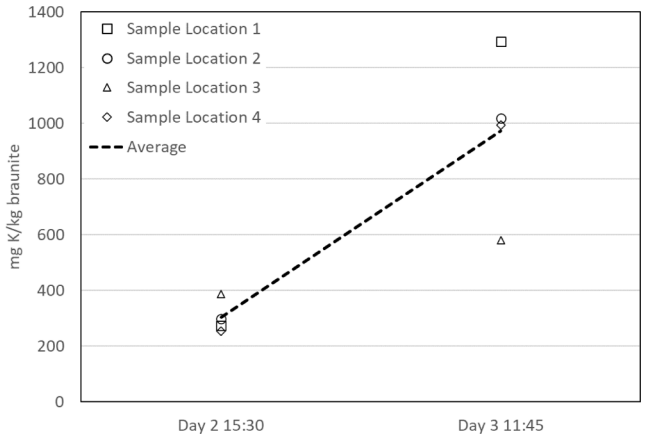


**Fig. 10.** Potassium content of braunite samples.

fuel alkalis was very low, and likely within the error margin of the elemental analysis results. For braunite, samples from four different locations in the reactor system were taken at two time points. Between these time points, the braunite inventory was exposed to approximately 137 g of fuel alkalis from approximately 2 h CLC operation with wood pellets, 1.5 h of CLC operation with wood char, and 1.25 h of operation with straw pellets. Potassium concentrations of the collected samples are shown in Fig. 10.

The average change in potassium concentration with an estimated reactor system inventory of 66 kg of braunite corresponds to 32% uptake of fuel alkalis by the braunite bed material. However, this calculated uptake figure is subject a large uncertainty due to the significant concentration spread between the four sample locations, and is likely underestimated due to the lack of detailed accounting of bed material added to and elutriated from the reactor system. For this reason, the calculated uptake figure should only be considered as a confirmation of significant uptake of alkalis by the bed material. Future experimental work will focus on refining the sampling, inventory accounting, and sample analysis procedures in order to reduce the error in such calculations.

Significant uptake of alkalis by ilmenite has been reported in previous CLC studies [7,8], as well as in investigations with ilmenite as a bed material for OCAC operation in a 12 MW boiler [24]. These studies attribute retention of alkalis in ilmenite to formation of K-titanate ($KTi_8O_{16}$) within the ilmenite particles. Although the alkali absorption capacity of ilmenite remains to be determined, potassium uptake equivalent of 1.5–2.0 wt% of ilmenite was reported at approximately 80 h of OCAC operation [23]. For the CLC experiments in the current study, alkali capture by K-titanate formation is likely to be significant, but may not be the only path for alkali retention. Ilmenite also contains species other than titanium that can be responsible for retaining alkalis in the oxygen carrier. Although many interactions are possible, the most likely elements to react with alkalis are Si, Mn and Al. Alkali silicates, and alkali aluminosilicates are well-known to be formed in combustion conditions [19], and the formation of potassium manganates can also be relevant [38].

Braunite oxygen carrier does not have an appreciable Ti content, eliminating the possibility for extensive formation of K-titanates. Alkali uptake by braunite can be explained by other elements found within the braunite OC that can form stable compounds with K at CLC conditions. Braunite is a Mn ore, with roughly 55 wt% Mn and 2.5 wt% Si content. An experimental study by Leion et al. [38] on the interaction of alkali ash components with Mn/Si-based oxygen carriers showed that $K_2CO_3$ is able to interact with Mn and Si, forming several species in both reducing and oxidative conditions. In this study, a sample of similar Mn to Si molar ratio, as found in the braunite OC, was found to form $K_2MnO_4$ in oxidative conditions and $K_2Mn_2O_3$ in reducing conditions. Alkali silicate formation was also detected. In light of this, formation of potassium manganates and alkali silicates is likely responsible for the alkali retention in the tests conducted with the braunite oxygen carrier.

The alkali-absorptive capabilities exhibited by both oxygen carriers may be a useful feature for biomass CLC technology. Absorption of alkalis by the oxygen carriers limits gas-phase alkali release and thus should be beneficial for avoiding fouling and corrosion of heat exchange surfaces which would be present in full-scale industrial implementations of CLC. However, the absorption capacity of both oxygen carriers, as well as potential effects of the absorbed alkalis on the bed material's reactivity or mechanical stability, remains to be determined. The relatively short operating times of the experimental campaign presented in this work do not allow for determination of such effects. Likewise, the results presented herein are not sufficient to determine advantages of each oxygen carrier for use with a particular fuel. Determination of long-term use effects and optimal oxygen carrier selection for different biomass types is deferred to future experimental campaigns that would require much longer operation times as well as an evaluation that includes consideration of reactivity, mechanical stability, cost, and alkali absorption capacity.

The third pathway for alkali retention in a condensed phase is the deposition of alkali species on internal surfaces of the reactor system. In

the current study such mechanisms are thought to be insignificant due to several factors. Firstly, significant losses to internal surfaces are known to occur due to physical deposition of alkali compounds on surfaces that are colder than typical operating temperatures of 800–900 °C [22]. In conventional fluidized bed boilers, such deposition occurs on steam tubes that are typically maintained at temperatures below 600 °C. In the current study, all internal surfaces are maintained above 800 °C, preventing condensation and deposition of most alkali compounds. Secondly, since the D-CFB system operates in the fast-fluidized regime, the majority of the internal surfaces are exposed to erosive conditions that would prevent significant deposit formation. Chemical bonding of alkali species to internal steel surfaces can occur in this reactor system but is expected to me minimal due to the low surface area to volume ratio of this relatively large pilot system.

### 4.5. AR alkali emissions

Another key observation from the results presented in Tables 3 and 4 is that AR alkali emissions are significant, although lower than in the FR. AR alkali emissions were also observed in previous alkali measurement campaigns in CLC [7,8], but the reason for their occurrence was never established. Since no fuel is fed into the AR during CLC operation, the alkalis that are eventually released to the gas phase of the AR, must be transported from the FR. One possibility is that alkali transport occurs as some unconverted fuel char is carried over to the FR with the oxygen carrier. Char carryover from the FR to the AR can be estimated form the carbon capture efficiency. Average carbon capture efficiency ($\eta_{oo\text{-}avg}$) figures for the conducted CLC test are summarized in Table 5. Test 2 operation was excluded as it did not represent true CLC operation (fuel was fed to the AR and well as the FR).

Table 5 results show that carbon capture efficiency during all CLC tests was low in operation with wood char fuel. This can be explained by this fuel's low volatiles content of 18.7 wt%. Unlike wood pellets and straw pellets fuels that loose >69% of their mass through spontaneous devolatilization in the FR, conversion of wood char to the gas phase, such that it can be oxidizable by the oxygen carrier, relies almost solely on char gasification. Since char gasification is much slower than devolatilization, wood char spends more time in the FR and has a greater chance to be conveyed to the AR by the circulating oxygen carrier material.

CLC operation with high-volatiles fuels, wood pellets and straw pellets, showed lower carbon capture efficiencies compared to typical values of >95% reported for high-volatiles fuels in CLC operation [7,8]. This indicates that the char that remains after devolatilization of the fuel, is partially conveyed to the AR. The carried over char burns in air in the AR and is detected with AR $CO_2$ concentration measurements. AR $CO_2$ is reflected in the calculation of carbon capture efficiency, as per Eq. (1). In conclusion, the apparent low carbon capture efficiency of the CLC tests indicates significant char carryover to the AR. This carryover and subsequent char combustion in the AR in the presence of air can explain the significant AR alkali emissions.

**Table 5**
CLC test average carbon capture efficiency.

| Test | Oxygen Carrier | Fuel | Period | $\eta_{oo\_avg}$ |
|---|---|---|---|---|
| **Test 1** | **Ilmenite** | **wood pellets (WP)** | 2 | 64% |
| **Test 3** | **Ilmenite** | **wood char (WC)** | 8 | 33% |
| **Test 4** | **Ilmenite** | **wood char (WC)** | 9 | 43% |
| **Test 5** | **Braunite** | **wood pellets (WP)** | 11 | 87% |
| | **Braunite** | **wood pellets (WP)** | 12 | 85% |
| | **Braunite** | **wood pellets (WP)** | 13 | 89% |
| **Test 6** | **Braunite** | **wood char (WC)** | 15 | 51% |
| **Test 7** | **Braunite** | **straw pellets (SP)** | 16 | 79% |

## 5. Conclusions

Online alkali emissions measurement with a surface ionization detector (SID) were carried out in a dual circulating fluidized bed chemical looping combustor. Oxygen carrier aided combustion (OCAC) and CLC tests were conducted with three different biomass fuels of varying alkali content (wood pellets, wood char, straw pellets), and two oxygen carrier materials (ilmenite, braunite). Results show that CLC operation results in higher gas-phase alkali release, when compared to OCAC operation. Analysis of the alkali release pathways applicable to the CLC process was conducted based on literature covering alkali release theory and alkali release experiments in combustion and gasification studies. This analysis and the experimental findings suggest that the higher gas-phase alkali release in CLC arises from the steam-rich conditions in the FR, where steam accelerates the decomposition of potassium salts to yield the release of alkalis as KOH(g) to the gas phase. Analysis of the alkali retention shows that >97% of the fuel alkalis are retained in the condensed phase in tests with ilmenite, while tests with braunite yield a retention >92%. Analysis of the retention pathways concludes that in CLC, up to 60–80% of the alkali retention can be attributed to the fuel ash formation process, while the residual amount of retention is caused by absorption of alkalis by the OC materials. For braunite, alkali retention was found to be likely caused by formation of alkali manganates and silicates. For ilmenite, alkali retention was found to be likely caused by formation of silicates, aluminosilicates, manganates, as well as through formation of alkali titanates. In CLC operation, AR gas-phase alkali emissions were found to be significant, but lower than those of the FR. It was concluded that AR alkali emissions arise from combustion of unconverted fuel that is carried over from the FR to the AR. Significant carryover was confirmed by low carbon capture efficiency of the conducted CLC tests.

## CRediT authorship contribution statement

**Ivan Gogolev:** Conceptualization, Methodology, Investigation, Validation, Formal analysis, Data curation, Visualization, Writing - original draft, Writing - review & editing. **Toni Pikkarainen:** Conceptualization, Methodology, Investigation, Validation, Formal analysis, Data curation, Writing - review & editing, Project administration. **Juho Kauppinen:** Conceptualization, Methodology, Investigation, Validation, Data curation. **Carl Linderholm:** Conceptualization, Supervision. **Britt-Marie Steenari:** Writing - review & editing. **Anders Lyngfelt:** Conceptualization, Writing - review & editing, Supervision, Project administration, Funding acquisition.

## Declaration of Competing Interest

The authors declare that they have no known competing financial interests or personal relationships that could have appeared to influence the work reported in this paper.

## Acknowledgements

This work was carried out with funding from Swedish Research Council, project "Biomass combustion chemistry with oxygen carriers", contract 2016-06023, and by the Swedish Energy Agency (grant number P43936-1).

## References

[1] Lyngfelt A, Leckner B, Mattisson T. A fluidized-bed combustion process with inherent CO2 separation; Application of chemical-looping combustion. Chem Eng Sci 2001;56:3101–13. https://doi.org/10.1016/S0009-2509(01)00007-0.
[2] Adánez J, Abad A. Chemical-looping combustion: Status and research needs. Proc Combust Inst 2019;37:4303–17. https://doi.org/10.1016/j.proci.2018.09.002.

[3] Lyngfelt A. Chemical Looping Combustion: Status and Development Challenges. Energy Fuels 2020;34:9077–93. https://doi.org/10.1021/acs.energyfuels.0c01454.
[4] Lyngfelt A, Thunman H. Construction and 100 h of Operational Experience of A 10-kW Chemical-Looping Combustor. Carbon Dioxide Capture Storage Deep Geol. Form., Elsevier 2005:625–45. https://doi.org/10.1016/B978-008044570-0/50122-7.
[5] Lyngfelt A, Brink A, Langørgen Ø, Mattisson T, Rydén M, Linderholm C. 11,000 h of chemical-looping combustion operation—Where are we and where do we want to go? Int J Greenh Gas Control 2019;88:38–56. https://doi.org/10.1016/j.ijggc.2019.05.023.
[6] Pachauri RK, Meyer L, Hallegatte France S, Bank W, Hegerl G, Brinkman S, et al. Climate Change 2014: Synthesis Report. Contribution of Working Groups I, II and III to the Fifth Assessment Report of the Intergovernmental Panel on Climate Change. Gian-Kasper Plattner 2014.
[7] Gogolev I, Soleimanisalim AH, Linderholm C, Lyngfelt A. Commissioning, performance benchmarking, and investigation of alkali emissions in a 10 kWth solid fuel chemical looping combustion pilot. Fuel 2020;119530. https://doi.org/10.1016/j.fuel.2020.119530.
[8] Gogolev I, Linderholm C, Gall D, Schmitz M, Mattisson T, Pettersson JBC, et al. Chemical-looping combustion in a 100 kW unit using a mixture of synthetic and natural oxygen carriers – Operational results and fate of biomass fuel alkali. Int J Greenh Gas Control 2019;88:371–82. https://doi.org/10.1016/j.ijggc.2019.06.020.
[9] Adánez-Rubio I, Abad A, Gayán P, De Diego LF, García-Labiano F, Adánez J. Biomass combustion with CO2 capture by chemical looping with oxygen uncoupling (CLOU). Fuel Process Technol 2014;124:104–14. https://doi.org/10.1016/j.fuproc.2014.02.019.
[10] Khan AA, de Jong W, Jansens PJ, Spliethoff H. Biomass combustion in fluidized bed boilers: Potential problems and remedies. Fuel Process Technol 2009;90:21–50. https://doi.org/10.1016/j.fuproc.2008.07.012.
[11] Baxter LL, Miles TR, Miles TR, Jenkins BM, Milne T, Dayton D, et al. The behavior of inorganic material in biomass-fired power boilers: Field and laboratory experiences. Fuel Process Technol 1998;54:47–78. https://doi.org/10.1016/S0378-3820(97)00060-X.
[12] Berguerand N, Lyngfelt A. Design and operation of a 10 kWth chemical-looping combustor for solid fuels - Testing with South African coal. Fuel 2008;87:2713–26. https://doi.org/10.1016/j.fuel.2008.03.008.
[13] Lyngfelt A, Linderholm C. Chemical-Looping Combustion of Solid Fuels - Status and Recent Progress. Energy Procedia 2017;114:371–86. https://doi.org/10.1016/j.egypro.2017.03.1179.
[14] Leion H, Mattisson T, Lyngfelt A. Solid fuels in chemical-looping combustion. Int J Greenh Gas Control 2008;2:180–93. https://doi.org/10.1016/S1750-5836(07)00117-X.
[15] Lyngfelt A. Chemical-looping combustion of solid fuels – Status of development. Appl Energy 2014;113:1869–73. https://doi.org/10.1016/j.apenergy.2013.05.043.
[16] Jenkins B, Baxter L, Miles Jr T, Miles T. Combustion properties of biomass. Fuel Process Technol 1998;54:17–46.
[17] Mims CA, Pabst JK. Alkali-catalyzed carbon gasification kinetics: Unification of H2O, D2O, and CO2 reactivities. J Catal 1987;107:209–20. https://doi.org/10.1016/0021-9517(87)90286-7.
[18] Keller M, Arjmand M, Leion H, Mattisson T. Chemical Engineering Research and Design Interaction of mineral matter of coal with oxygen carriers in chemical-looping combustion (CLC). Chem Eng Res Des 2013;92:1753–70. https://doi.org/10.1016/j.cherd.2013.12.006.
[19] Zevenhoven M, Yrjas P, Hupa M. Ash-Forming Matter and Ash-Related Problems. Handb. Combust., Weinheim, Germany: Wiley-VCH Verlag GmbH & Co. KGaA; 2010, p. 493–531. doi:10.1002/9783527628148.hoc068.
[20] Wellinger M, Biollaz S, Wochele J, Ludwig C. Sampling and online analysis of alkalis in thermal process gases with a novel surface ionization detector. Energy Fuels 2011;25:4163–71. https://doi.org/10.1021/ef200811q.
[21] Davidsson KO, Elled A-L, Eskilsson D, Leckner B, Åmand L-E, Steenari B-M. Countermeasures against alkali-related problems during combustion of biomass in a circulating fluidized bed boiler. Chem Eng Sci 2008;63:5314–29. https://doi.org/10.1016/j.ces.2008.07.012.
[22] Hupa M, Karlström O, Vainio E. Biomass combustion technology development - It is all about chemical details. Proc Combust Inst 2017;36:113–34. https://doi.org/10.1016/j.proci.2016.06.152.
[23] Gyllén A. Oxygen carrier aided combustion: Implementation of oxygen carriers to existing industrial settings. Chalmers University of Technology 2019.
[24] Corcoran A, Marinkovic J, Lind F, Thunman H, Knutsson P, Seemann M. Ash properties of ilmenite used as bed material for combustion of biomass in a circulating fluidized bed boiler. Energy Fuels 2014;28:7672–9. https://doi.org/10.1021/ef501810u.
[25] Wiinikka H, Grönberg C, Öhrman O, Boström D. Influence of TiO2 additive on vaporization of potassium during straw combustion. Energy Fuels 2009;23:5367–74. https://doi.org/10.1021/ef900544z.
[26] Davidsson KO, Engvall K, Hagström M, Korsgren JG, Lönn B, Pettersson JBC. A surface ionization instrument for on-line measurements of alkali metal components in combustion: Instrument description and applications. Energy Fuels 2002;16:1369–77. https://doi.org/10.1021/ef020020h.
[27] Tran K-Q, Iisa K, Hagström M, Steenari B-M, Lindqvist O, Pettersson JBC. On the application of surface ionization detector for the study of alkali capture by kaolin in a fixed bed reactor. Fuel 2004;83:807–12. https://doi.org/10.1016/J.FUEL.2003.10.014.
[28] Davidsson KO, Korsgren JG, Pettersson JBC, Jäglid U. The effects of fuel washing techniques on alkali release from biomass. Fuel 2002;81:137–42. https://doi.org/10.1016/S0016-2361(01)00132-6.
[29] Pushp M, Gall D, Davidsson K, Seemann M, Pettersson JBC. Influence of Bed Material, Additives, and Operational Conditions on Alkali Metal and Tar Concentrations in Fluidized Bed Gasification of Biomass. Energy Fuels 2018;32:6797–806. https://doi.org/10.1021/acs.energyfuels.8b00159.
[30] Jensen PA, Frandsen FJ, Dam-Johansen K, Sander B. Experimental Investigation of the Transformation and Release to Gas Phase of Potassium and Chlorine during Straw Pyrolysis 2000. doi:10.1021/ef000104v.
[31] Johansen JM, Jakobsen JG, Frandsen FJ, Glarborg P. Release of K, Cl, and S during pyrolysis and combustion of high-chlorine biomass. Energy Fuels 2011;25:4961–71. https://doi.org/10.1021/ef201098n.
[32] Tchoffor PA, Davidsson KO, Thunman H. Transformation and Release of Potassium, Chlorine, and Sulfur from Wheat Straw under Conditions Relevant to Dual Fluidized Bed Gasification 2013. doi:10.1021/ef401703a.
[33] Knudsen JN, Jensen PA, Dam-Johansen K. Transformation and release to the gas phase of Cl, K, and S during combustion of annual biomass. Energy Fuels 2004;18:1385–99. https://doi.org/10.1021/ef049944q.
[34] Dayton DC, French RJ, Milne TA. Direct Observation of Alkali Vapor Release during Biomass Combustion and Gasification. 1. Application of Molecular Beam/Mass Spectrometry to Switchgrass Combustion. vol. 9. 1995.
[35] Novaković, AN, Van Lith SC, Frandsen FJ, Jensen PA, Holgersen LB. Release of Potassium from the Systems K-Ca-Si and K-Ca-P † n.d. doi:10.1021/ef8010417.
[36] Hildor F, Zevenhoven M, Brink A, Hupa L, Leion H. Understanding the Interaction of Potassium Salts with an Ilmenite Oxygen Carrier under Dry and Wet Conditions. ACS Omega 2020. https://doi.org/10.1021/acsomega.0c02538.
[37] van Lith SC, Jensen PA, Frandsen FJ, Glarborg P. Release to the gas phase of inorganic elements during wood combustion. Part 2: Influence of fuel composition. Energy Fuels 2008;22:1598–609. https://doi.org/10.1021/ef060613i.
[38] Henrik Leion, Pavleta Knutsson B-MS. Experimental Evaluation of Interactions between K, Ca, And P And Mn/Si-Based Oxygen Carriers. Eur. Biomass Conf. Exhib. Proc. Vol. 2017, Issue 25th EUBCE, June 2017, 2017, p. 660–5.